NANO LETTERS

2003
Vol. 3, No. 9
1273−1277

# Generalized Chemical Reactivity of Curved Surfaces: Carbon Nanotubes

**Seongjun Park,[†] Deepak Srivastava,[‡] and Kyeongjae Cho*[,§]**

*Departments of Chemical and Mechanical Engineering, Stanford University, Stanford, California 94305, and NASA Ames Research Center, CSC/NAS, Mail Stop 229-1, Moffett Field, California 94035-1000*

*Received May 1, 2003; Revised Manuscript Received July 17, 2003*

**ABSTRACT**

**We have developed a model to predict the chemical reactivity of carbon nanotubes (CNTs) quantitatively from their initial structures. The parameters, universal for each reaction, of the model can be obtained from a graphene sheet analysis. The chemical reactivity of hydrogenation, hydroxylation, and fluorination were predicted within 0.1–0.3 eV errors, compared with first principle simulation results. The model also predicted the enhanced chemical reactivity of mechanically bent CNTs. The predictions can be applied to the controlled functionalization of CNTs.**

On the basis of carbon nanotubes (CNTs),[1] many potential nanoelectronic devices have been proposed and investigated. Some of them, such as p−n junctions[2] and gas sensors,[3] are based on the direct chemical interactions between external chemical species and CNTs. Others, such as chemical and biosensors,[4,5] are based on adsorbate-mediated interactions. These devices are based on chemical reactions on CNTs. Recently, the fluorination of the side walls of CNTs[6] and further derivations[7,8] were demonstrated. Also, the interactions between the side walls and radicals were studied using molecular dynamics.[9,10] Although a few limited reactions have been demonstrated on CNT surfaces, more controlled reactions are required for general applications. For example, selective doping of p−n junctions and an enhanced reaction between an inert CNT and adsorbates for adsorbates-mediated sensors are necessary. In addition, in a recent demonstration, it was shown that CNTs can function as a nanogate through wiring their appropriate positions.[11] Thus, a detailed understanding of the chemical reactivity on curved CNT surfaces is desired.

In general, the chemical reactivity of a CNT is governed by the local atomic structure.[12] For example, the inherently curved surface of a CNT has different chemical reactivity from the planar sheets of graphene layers. On the basis of this idea, it has been shown that the conformational deformation in a CNT can enhance the hydrogenation energy at the location of the excess deformation so that it is possible to change the chemical reactivity of a CNT by mechanical deformation.[13,14] To functionalize a CNT as desired, however, we need an analytical model for the quantitative dependence of the chemical reactivity on the local atomic structure of a CNT. Therefore, we have studied the local chemical reactivity of a CNT to predict the chemical reactivity for the given deformation.

Among the various types of chemical reactions, we first focused on single covalent bond reactions as representative systems, for example, hydrogenation (−H),[9] fluorination (−F),[6] methoxylation (−OR),[7] and alkylation (−R).[8] In those reactions, an external reactant X makes a bond with a C atom, which is strained to increase its bond order. Thus, the reaction can be conceptually decomposed in the following way: (a) straining a C atom to form $sp^3$ hybridization with fixed neighbors, (b) breaking the $\pi$ bonds of the strained C atom with the neighboring C atoms, (c) binding the free $\pi$ orbital with X, and (d) relaxing the neighboring C atoms to accommodate the changes in bonding character after the reaction. The analysis can be further simplified by combining b and c into a single event of the bonding of X on a locally strained C atom, as depicted in Figure 1a.

Following the decomposition, the total reaction energy $E_{total}$, which is the index of chemical reactivity, can be divided into three terms: strain energy $E_{strain}$, C−X binding energy $E_{C-X}$, and global relaxation energy $E_{relax}$. $E_{strain}$ is universal because no external reactant is introduced. It is also always positive because energy is absorbed during the straining process. However, $E_{C-X}$ depends on X and should be negative for the reaction to occur.

We have developed analytic expressions for the individual energy terms as functions of pyramidal angle $\theta_p$,[12] an indication of local atomic structure as shown in Figure 1b on the basis of the analysis of a graphene sheet, which is a good analogue of large-radius CNTs. They were parametrized using the total energy pseudopotential density functional

* Corresponding author. E-mail: kjcho@stanford.edu.
[†] Department of Chemical Engineering, Stanford University.
[‡] NASA Ames Research Center.
[§] Department of Mechanical Engineering, Stanford University.

10.1021/nl0342747 CCC: $25.00 
**Published on Web 07/31/2003**

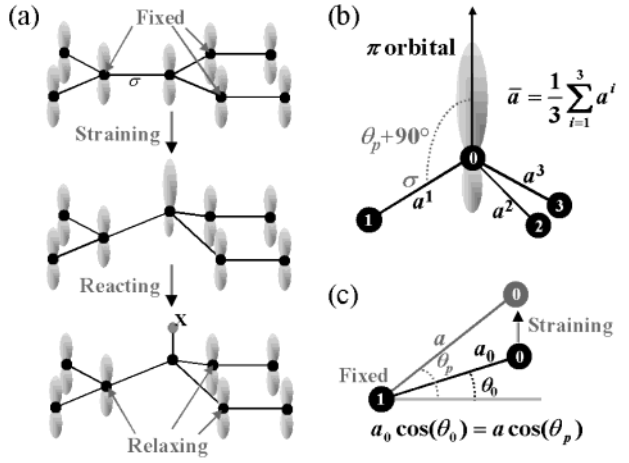


**Figure 1.** (a) Decomposition of a reaction on a graphene sheet. (b) Pyramidal angle $\theta_p$ is defined by the angle between the $\pi$ orbital and $\sigma$ bond minus 90° so that $\theta_p = 0°$ for a graphene sheet and $\theta_p = 19.47°$ for $sp^3$. For practical reasons, we take the average of three $\theta_p$values. (c) Relationship between $\theta_p$ and $a$.

**Table 1.** Initial Equilibrium Pyramidal Angles $\theta_0$ (deg) and Radius $R$ (Å) of CNTs

| | graphite | 15, 0 | 13, 0 | 12, 0 | 10, 0 | 9, 0 | 8, 0 | 6, 0 | 5, 0 | $C_{60}$ |
|---|---|---|---|---|---|---|---|---|---|---|
| $\theta_0$ | 0.00 | 3.43 | 3.97 | 4.30 | 5.12 | 5.78 | 6.41 | 8.54 | 9.96 | 11.55 |
| $R$ | ∞ | 5.84 | 5.07 | 4.68 | 3.91 | 3.53 | 3.15 | 2.39 | 1.95 | 3.54 |

theory (DFT).[15] We have tested the accuracy of the models with (10, 0) CNT and $C_{60}$ fullerene and have verified that the models provide a good description for 1D and 2D deformations of a graphene sheet as well as a CNT and a fullerene. Finally, according to the models, we derived an equation to predict $E_{total}$ from the initial structure of a CNT. This equation was applied to various CNTs, of which $\theta_p$ values are listed in Table 1. The predicted $E_{total}$ values were compared with fully relaxed DFT results.[16]

We performed DFT simulation using DFT++[17] and VASP (Vienna Ab-initio Simulation Package).[18] During DFT simulations, the cutoff energy was over 26 Ry, and periodic boundary conditions were applied with at least 5-Å vacuum separations between CNTs or graphene sheets. After a $k$-point convergence test, we chose single $k$-point sampling with 16 unit cells for graphene sheets and 6 $k$-points with a single unit cell for CNTs. We also use single $k$-point sampling for $C_{60}$. During geometry optimizations, the atomic positions were relaxed until the forces were less than 0.05 eV/Å.

**Strain Energy.** $E_{strain}$ is defined as the excess energy in the system as a C atom at equilibrium is pulled up to form $sp^3$ hybridization while all the other C atoms are held fixed.[19] $E_{strain}$ thus is composed of the bond-bending energy of four C atoms—the pulled-up C atom and its three nearest neighbors—and the bond-stretching energy of three bonds. It can be described by force constant models in terms of $\theta_p$ and bond length a with their initial equilibrium values, $\theta_0$'s and $a_0$'s.

$$E_{strain} = \frac{1}{2}k_b\sum_{i=0}^{3}(\theta_p^i - \theta_0^i)^2 + \frac{1}{2}k_s\sum_{i=1}^{3}(a_p^i - a_0^i)^2 \qquad (1)$$

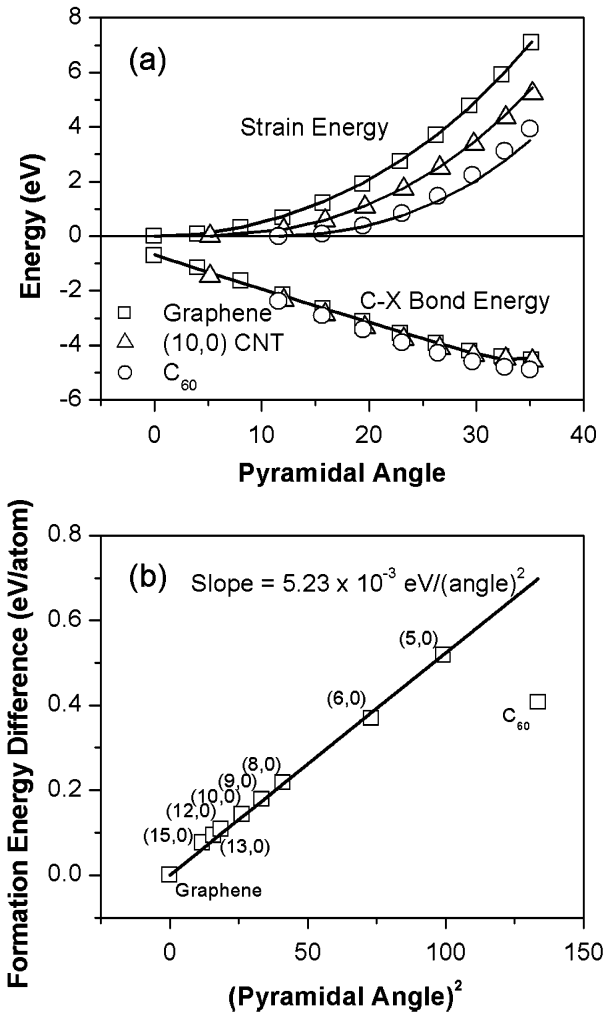


**Figure 2.** (a) $E_{strain}$ and $E_{C-X}$. The black curves are fitted curves to eqs 2 and 6. The gray curves are estimated $E_{strain}$ values from eq 2. (b) Formation-energy difference between CNTs and a graphene sheet.

$\Delta\theta_p^i (i = 1-3) \cong \Delta\theta_p^0/3$ because only one of the three bonds of each first-nearest-neighbor C atom is bent. $\Delta a$ can be expressed in terms of $\theta_p$, as shown in Figure 1c. Thus, eq 1 can be simplified as a function of $\theta_p$ only.

$$E_{strain} = \frac{2}{3}k_b(\theta_p - \theta_0)^2 + \frac{3}{2}k_s\bar{a}^2\left(\frac{\cos\theta_0}{\cos\theta_p} - 1\right)^2 \qquad (2)$$

A set of $E_{strain}$ values for a graphene sheet, a (10, 0) CNT, and a $C_{60}$ fullerene were computed with the DFT method and are shown in Figure 2a. The computed $E_{strain}$ values of the graphene sheet were fitted to eq 2 and gave the universal parameters $k_b$ and $k_s$ as 7.51‰ × $10^{-3}$ eV/(angle)$^2$ and 8.30 eV/Å$^2$, respectively. We examined eq 2 and the parameters as predicting $E_{strain}$'s of the (10, 0) CNT and the $C_{60}$ fullerene. Figure 2a shows that the predicted $E_{strain}$ values and the fully relaxed DFT values are in good agreement up to $\theta_p = 25°$, within which most chemical reactions on CNT surfaces can be described.

**C−X Binding Energy.** $E_{C-X}$ is the binding energy of X on locally strained C atom and comprises two terms: the

breaking of $\pi$ bonds into a free $\pi$ orbital and the binding of the free $\pi$ orbital with X. For the first term, the $\pi$ bond-breaking energy of a graphene sheet $E_{graph}$ is taken as the reference, and an energy shift $E_{shift}$ due to the inherent curvature of a CNT is subtracted as eq 3. The formation-energy difference $\Delta E_f$ between CNTs and a graphene sheet comes from the strain of $\sigma$ bonds and $E_{shift}$. Hence, $E_{shift}$ can be described by a certain portion of $\Delta E_f$. We computed $\Delta E_f$ of CNTs and summarized the results in Figure 2b. $\Delta E_f$ is a function of $\theta_0^2$ with a constant $\alpha = 5.23 \times 10^{-3}$ eV/(angle)$^2$. For the first approximation, we chose the portion as 1. Because of the small value of $\alpha$, however, $E_{first}$ is insensitive to the portion unless a CNT is (6, 0) or smaller. We also compared the computed $\Delta E_f$ of $C_{60}$ with the value calculated from experimental data, formation energies of $C_{60}$,[20] and a graphene sheet,[21] and we found that the computed $\Delta E_f$ of $C_{60}$ is within 2% error.

$$E_{first}(\theta_0) = E_{graphite} - \alpha {\theta_0}^2 \quad (3)$$

For the second term, the rehybridization due to local straining can be expressed by the portion of s and p orbitals as eq 4 from the $\pi$-orbital axis vector analysis.[22] According to eq 4, the $\pi$ orbital is between the two limiting configurations and is also a function of $\theta_p$. $sp^2 + p$ represents a graphite-like structure with $\theta_p = 0°$ and has a p orbital for $\pi$ orbital. At the other extreme, $p^3 + s$ has an s orbital for a $\pi$ orbital with the maximum of $\theta_p = 35.26°$.

$$|\pi\rangle = \sqrt{2}\tan(\theta_p)|s\rangle + \sqrt{1 - 2\tan^2(\theta_p)}|p\rangle \quad (4)$$

The second energy term can be estimated from the expectation value of the Hamiltonian $H$ between the $\pi$ orbital state in eq 4 and a state $\langle x|$ of X.

$$E_{second}(\theta_p) = \sqrt{2}\tan(\theta_p)E_{sx} + \sqrt{1 - 2\tan^2(\theta_p)}E_{sx} \quad (5)$$

where $E_{sx}$ and $E_{px}$ are $\langle s|H|x\rangle$ and $\langle p|H|x\rangle$, respectively. $E_{sx}$ and $E_{px}$ depend only on the species of X so that they can be treated as constants for the given X. $E_{sx}$ is generally larger than $E_{px}$ because the eigenvalue of the s orbital is larger than that of the p orbital.

Combining eqs 3 and 5, $E_{C-X}$ can be written as eq 6, which is a function of only $\theta_p$ with $E_{shift}$.

$$E_{C-X}(\theta_p) = E_{graphite} - \alpha\theta_0^2 + \sqrt{2}\tan(\theta_p)E_{sx} + \sqrt{1 - 2\tan^2(\theta_p)}E_{sx} \quad (6)$$

The dependence of $E_{C-X}$ on $\theta_p$ was examined by a set of hydrogenation-energy calculations on the strained C atoms. During the simulations, all of the C atoms were held fixed to maintain $\theta_p$, and the position of the H atom was relaxed. The parameters, $E_{sx}$, $E_{px}$, and a constant $E_{graphite}$ were obtained by fitting the calculated $E_{C-X}$ values of a graphene sheet to eq 6, as shown in Figure 2a. $E_{graphite}$ is 0.58 eV, and the parameters are listed in Table 2. $E_{C-X}$ behaves almost linearly on $\theta_p$ because $\tan(\theta_p) \cong \theta_p$ for small angles and the last term of eq 6 changes gradually with $\theta_p$.

**Table 2.** $E_{sx}$ and $E_{px}$ and the Maximum Errors Compared to DFT Results in Figure 3

| | $E_{sx}$ (eV) | $E_{px}$ (eV) | error in $E_{total}$ (eV) | error in $\theta_p^{min}$ (deg) |
|---|---|---|---|---|
| CNT−H | −5.15 | −1.31 | 0.1 | 2 |
| CNT−OH | −5.27 | −1.11 | 0.2 | 2 |
| CNT−F | −5.22 | −2.10 | 0.3 | 1 |

Figure 2a also shows that $E_{C-X}$'s of a (10, 0) CNT and a $C_{60}$ fullerene agree with the graphene sheet data with small $E_{shift}$ values. In addition, we note that the C−H bond length is a function of $\theta_p$ only and is independent of the original structure, varying between 1.09 and 1.22 Å. These results verify the underlying basis of eq 6 that the nature of the C−H bond depends mainly on $\theta_p$. Hence, $E_{C-X}$ is a function of local $\theta_p$ only with small $E_{shift}$ values.

**Global Relaxation Energy.** $E_{relax}$ comes from the relaxation of the first nearest neighbors because of their strain after the reaction. Thus, the final structure, $\theta_p^{min}$, of the reacting C atom can be determined at the minimum of the sum of $E_{strain}$ and $E_{C-X}$ only, as eq 7. The corresponding energy is $E_{total} - E_{relax}$. Comparing this value with $E_{total}$ of a fully relaxed configuration with the DFT method,[16] $E_{relax}$ was found to be $-0.2 \pm 0.05$ eV for a graphene sheet, a (10, 0) CNT, and a $C_{60}$ fullerene so that the variation in $E_{relax}$ on the initial structure remains within 0.05 eV. Thus, $E_{relax}$ can be taken to be $-0.2$ eV regardless of the initial structure.

$$\left.\frac{d(E_{strain}(\theta_p) + E_{C-X}(\theta_p))}{d\theta_p}\right|_{\theta_p=\theta_p^{min}} = 0 \quad (7)$$

When all three energy terms are combined, the model, which can predict $E_{total}$ as well as $\theta_p^{min}$, with two parameters $E_{sx}$ and $E_{px}$ is completed.

$$E_{total} = E_{strain}(\theta_p^{min}) + E_{C-X}(\theta_p^{min}) + E_{relax}$$

For the purpose of the validation and application of the model, $E_{total}$ values were predicted for hydrogenation, hydroxylation, and fluorination on various CNT surfaces. Parameters $E_{sx}$ and $E_{px}$ for hydroxylation (−OH) and fluorination were deduced from the graphene sheet analysis following the similar procedure of hydrogenation. Figure 3 shows that the model can predict $\theta_p^{min}$ and $E_{total}$ values within small errors compared to DFT results. The parameters and the error ranges are summarized in Table 2. The larger error in the hydrogenation energy of a $C_{60}$ fullerene is mainly due to $E_{shift}$. A $C_{60}$ fullerene is more stable than the CNT of a comparable radius. $E_{total}$ for a $C_{60}$ fullerene (Figure 2b) is thus smaller than the CNT-based estimated value.

We noted from Figure 3 that metallic CNTs are slightly more reactive than the semiconducting CNTs and that the reactivity difference is larger for the fluorinations. Also, the

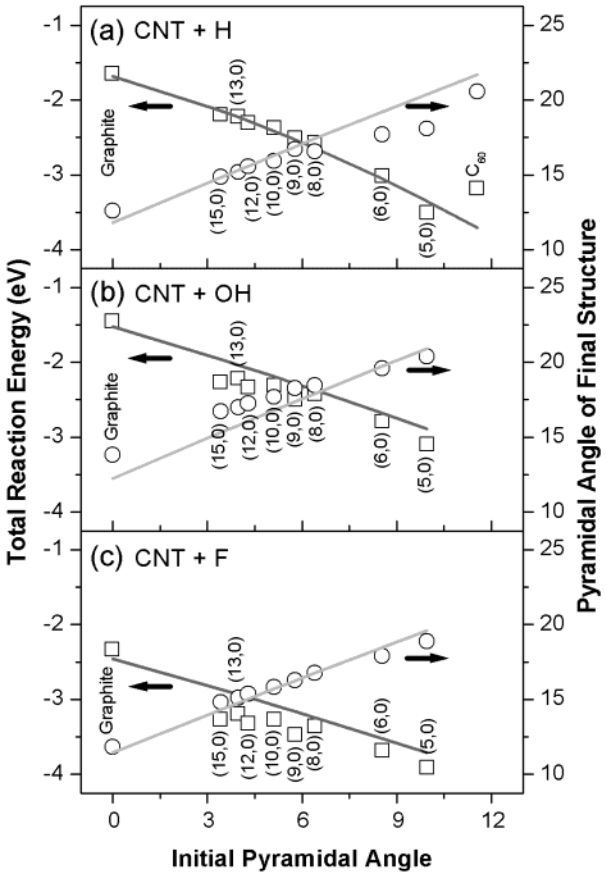


**Figure 3.** DFT-computed $E_{total}$ (□) and $\theta_p^{min}$ values (○) for fully relaxed configurations and their estimated values (solid curves) for (a) hydrogenation, (b) hydroxylation, and (c) fluorination.

errors in $E_{total}$ are larger for fluorination. We believe that they are due to the electron affinity difference between X and CNTs. In other words, this model works better when the bond has more covalent character.

The decomposition of $E_{total}$ provides a better understanding of the chemical reactivity of CNTs. Because $E_{relax}$ is relatively small, $E_{total}$ is determined by two competing terms: $E_{strain}$ and $E_{C-X}$. When the negative $E_{C-X}$ dominates, the reaction occurs at the minimum of their sum. In addition, the trend in the $E_{total}$ curve can be understood by the behaviors of the two major energy terms. $E_{strain}$ curves are nearly identical but shifted with respect to the graphene sheet curve by $\theta_0$ values, whereas the $E_{C-X}$ curve is almost linear and independent of the initial structure (Figure 2a). Thus, $E_{total}$, the sum of the energy terms, behaves almost linearly with $\theta_0$. The linear behavior of $E_{total}$ can be confirmed by another report.[14]

Finally, the model was applied to the chemical reactivity prediction of mechanically deformed CNTs. Because eq 2 of $E_{strain}$ and eq 6 of $E_{C-X}$ depend only on $\theta_p$ of the reacting C atom, the model can be extended to the chemical reactivity prediction of conformationally deformed CNTs. As an example, we examined bent CNTs. First, the configurations of 0−40° bent (10, 0) CNTs were prepared by molecular dynamics simulations using the Tersoff−Brenner potential for C−C interactions.[23] We then predicted the hydrogenation energies of each C atom from its $\theta_p$ and the developed model.

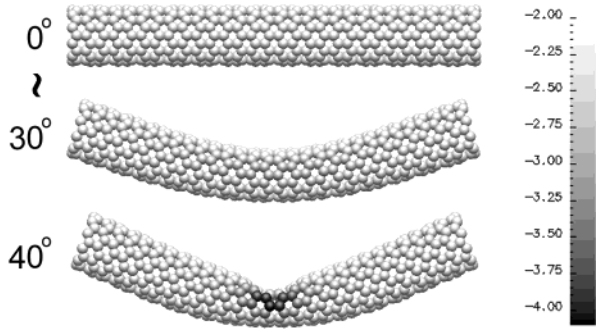


**Figure 4.** Chemical reactivity (hydrogenation energy) change as a function of bending angle.

The results in Figure 4 show that the local chemical reactivity of CNTs can be controlled by proper mechanical deformations, which can be predicted by the developed model. In Figure 4, no significant change but the gradual increase in hydrogenation energies of C atoms around the center of the CNT from −2.2 to −2.6 eV was observed up to 30°; however, a dramatic enhancement at the bent area is noted at 40° because the hydrogenation energies of six C atoms on each side exceeded −3.6 eV. In other words, we need greater than 40° bending to enhance the chemical reactivity of hydrogenation significantly in a certain area. The enhanced hydrogenation energy in the kink area is in agreement with other recent work.[13,14]

In summary, a generalized model with two parameters for $E_{total}$ of CNTs has been formulated as a function of local $\theta_p$ only. Parameters $E_{sx}$ and $E_{px}$ of each reaction are readily computable by a set of calculations on a graphene sheet. As examples, $E_{total}$ values were predicted for the hydrogenation hydroxylation and fluorination of various CNTs. As an example of controlling chemical reactivity, the model predicted enhanced hydrogenation energy at the kink site of bent CNTs. The model could be useful in rapid prototyping of the chemical reactivity. The approach can be extended to multibond and other bond-type reactions.

**Acknowledgment.** This research is supported by a NASA Ames Director's Discretionary Fund (DDF) Award to D.S. and K.C. D.S. is supported by NASA contract 755-30-11 to CSC. The DFT simulations are performed under NPACI allocation SUA239 "Nanoscale Materials Simulations".

## References

(1) Iijima, S. *Nature* **1991**, *354*, 56−58.
(2) Zhou, C. W.; Kong, J.; Yenilmez, E.; Dai, H. *Science* **2000**, *290*, 1552−1555.
(3) Kong, J.; Franklin, N. R.; Zhou, C. W.; Chapline, M. G.; Peng, S.; Cho, K.; Dai, H. *Science* **2000**, *287*, 622−625.
(4) Wong, S. S.; Joselevich, E.; Woolley, A. T.; Cheung, C. L.; Lieber, C. M. *Nature* **1998**, *394*, 52−55.
(5) Chen, R. J.; Zhang, Y.; Wang, D.; Dai, H. *J. Am. Chem. Soc.* **2001**, *123*, 3838−3839.
(6) Mickelson, E. T.; Huffman, C. B.; Rinzler, A. G.; Smalley, R. E.; Hauge, R. H.; Margrave, J. L. *Chem. Phys. Lett.* **1998**, *296*, 188−194.
(7) Mickelson, E. T.; Chiang, I. W.; Zimmerman, J. L.; Boul, P. J.; Lozano, J.; Liu, J.; Smalley, R. E.; Hauge, R. H.; Margrave, J. L. *J. Phys. Chem. B* **1999**, *103*, 4318−4322.
(8) Boul, P. J.; Liu, J.; Mickelson, E. T.; Huffman, C. B.; Ericson, L. M.; Chiang, I. W.; Smith, K. A.; Colbert, D. T.; Hauge, R. H.; Margrave, J. L.; Smalley, R. E. *Chem. Phys. Lett.* **1999**, *310*, 367−372.

(9) Ma, Y. C.; Xia, Y. U.; Zhao, M. W.; Ying, M. J.; Liu, X. D.; Liu, P. J. *J. Chem. Phys.* **2001**, *115*, 8152−8156.
(10) Ni, B.; Sinnott, S. B. *Phys. Rev. B* **2000**, *61*, R16343−R16346.
(11) Bachtold, A.; Hadley, P.; Nakanishi, T.; Dekker, C. *Science* **2001**, *294*, 1317−1320.
(12) Haddon, R. C. *Science* **1993**, *261*, 1545−1550.
(13) Srivastava, D.; Brenner, D. W.; Schall, J. D.; Ausman, K. D.; Yu, M. F.; Ruoff, R. S. *J. Phys. Chem. B* **1999**, *103*, 4330−4337.
(14) Gulseren, O.; Yildirim, T.; Ciraci, S. *Phys. Rev. Lett*. **2001**, *87*, 116802.
(15) See for the review of the DFT method Payne, M. C.; Teter, M. T.; Allan, D. C.; Arias, T. A.; Joannopoulos, J. D. *Rev. Mod. Phys*. **1992**, *64*, 1045−1097.
(16) C atoms up to the third nearest neighbors for graphite, the first nearest neighbors for CNTs, and all for $C_{60}$ were relaxed for the fully relaxed simulations.
(17) Ismail-Beigi, S.; Arias, T. A. *Comput. Phys. Commun*. **2000**, *128*, 1−45.
(18) Kresse, G.; Furthmuller, J. *Comput. Mater. Sci*. **1996**, *6*, 15−50. Kresse, G.; Furthmuller, J. *Phys. Rev. B* **1996**, *54*, 11169−11186.
(19) Fixed neighbors are a reasonable approximation because the bond length of a graphene sheet at $\theta_p = 19.47°$ is 1.51 Å and it is 1.54 Å for $sp^3$ hybridization.
(20) Steele, W. V.; Chirico, R. D.; Smith, N. K.; Billups, W. E.; Elmore, P. R.; Wheeler, A. E. *J. Phys. Chem.* **1992**, *96*, 4731−4733.
(21) Girifalco, L. A.; Lad, R. A. *J. Chem. Phys*. **1956**, *25*, 693−697.
(22) One s and three p orbitals are assigned to three $\sigma$ bonds and one $\pi$ orbital, according to Haddon, R. C. *Acc. Chem. Res.* **1988**, *21*, 243−249.
(23) Brenner, D. W. *Phys. Rev. B* **1990**, *42*, 9458−9471.

NL0342747